ISBN: 978-3-95450-215-8 ISSN: 2226-0366 doi:10.18429/JACoW-LINAC2022-MOPORI06

IMPROVEMENTS ON THE MODIFIED NOMARSKI INTERFEROMETER FOR MEASUREMENTS OF SUPERSONIC GAS JET DENSITY PROFILES

C. Swain*, J. Wolfenden, A. Salehilashkajani, H D. Zhang, O. Apsimon, C. P. Welsch
Cockcroft Institute, Daresbury Laboratory, Warrington, UK
University of Liverpool, Liverpool, UK

Abstract

For supersonic gas jet based beam profile monitors such as that developed for the High Luminosity Large Hadron Collider (HL-LHC) upgrade, density profile is a key characteristic. Due to this, non-invasive diagnostics to study the jet's behaviour have been designed. A Nomarski interferometer was constructed to image jets 30 µm to 1 mm in diameter and study changes in their density. A microscope lens has been integrated into the original interferometer system to capture phase changes on a much smaller scale than previous experiments have achieved. This contribution presents the optimisation and results gained from this interferometer.

INTRODUCTION

The use of supersonic gas jets is becoming more common within accelerator facilities, meaning it is important that suitable diagnostics are developed to properly characterise them. An example of this is the beam gas curtain (BGC) currently under development by the Cockcroft Institute (CI), CERN, and GSI. The BGC is a non-invasive beam profile monitor being developed for installation on the HL-LHC [1], and is designed for use on both the proton beam and hollow electron lens (HEL) [2, 3]. There are two working principles for the BGC, beam induced fluorescence (BIF) [4], and ionisation profile monitoring (IPM) [5]. In both operating modes, results are proportional to the density profile of the gas jet, making this an important property which must be properly understood to allow for accurate measurements. Whilst density distributions of the jet have been simulated [5], measured values for comparison and validation are still needed. Therefore, a diagnostic setup has been designed and tested at CI for this purpose. A modified Nomarski interferometer [6] was chosen to provide non-invasive imaging from which the density profile could be attained. Utilising a single optical path and compact design, this style of interferometry was chosen due to its benefits over other systems [7, 8]. An example of one such benefit is that the single path length allows for reductions in the alignment requirements and susceptibility to instability shown by split path interferometers, such as the Mach Zender system [9]. This paper presents updates to the system previously developed at CI [10], including the integrated microscope, new measurements, and possible improvements to be made.

* Catherine.Swain@liverpool.ac.uk

INTERFEROMETRY THEORY

Interferometry relies on the interference of coherent light sources creating fringes which can be imaged. From these images, or interferograms, properties of the media the light has propagated through can be found through studying changes in phase shift. In this interferometry system, a Wollaston prism was used to create the interferograms. The prism is made of birefringent material, in this case magnesium fluoride. Two triangular prisms are fit together with orthogonal optical axes, creating a polarising beam splitter with a fixed opening angle between the resulting rays [11]. A linearly polarised laser which is passed through the prism will diverge into an ordinary and extraordinary ray as it crosses the centre axes, as shown in Fig. 1.

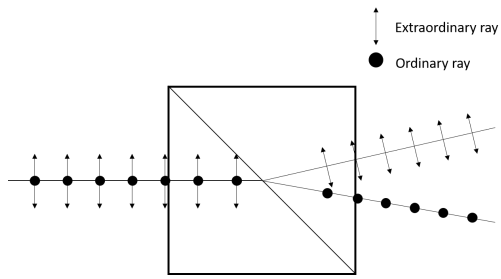

Figure 1: Diagram of Wollaston prism showing how light is split as it crosses the optical axis.

A focusing lens is used to focus the two rays into an interferogram, from which the phase shift they have undergone can be observed. These changes in phase shift can be directly linked to density gradients the laser has experienced via the Lorentz-Lorenz equation (Eq. 1). For gases with a density of less than 10^{19} cm^{-3}, it can be assumed that the refractive index (η) is close to 1. Therefore, Eq. (1) gives an approximation for the density [12]

$$\rho \approx (\eta - 1)\frac{2}{3}\frac{N_A}{A} \tag{1}$$

where density is given in m^{-3}, N_A is Avogadro's constant (6.022×10^{23} mol^{-1}), and A is the molar refractivity (for nitrogen, used in this study, A = 4.46 m^3 mol^{-1} [13]). This equation can then be used to form a relationship between density and phase shift, as given in Eq. (2) [12]

$$\Delta\phi = l\frac{3\pi}{\lambda}\frac{A}{N_A}\rho \tag{2}$$

where l is the laser path length through the media and λ is the laser wavelength. In this study l was taken as being equal

ISBN: 978-3-95450-215-8 ISSN: 2226-0366 doi:10.18429/JACoW-LINAC2022-MOPORI06

to the diameter of the gas jet nozzle throat, although due to free jet expansion, realistically it would be larger [14]. By using these two equations, a density profile of the gas jet could be constructed from an interferogram.

EXPERIMENTAL SET UP

A 532 nm laser was propagated through a polariser and beam expander, then into the vacuum chamber where gas jets were produced. The beam expander was added to the system as it allowed for the reduction of irregularities that were introduced to interferograms by the Gaussian beam profile. These optics upstream of the experimental chamber are shown in Fig. 2.

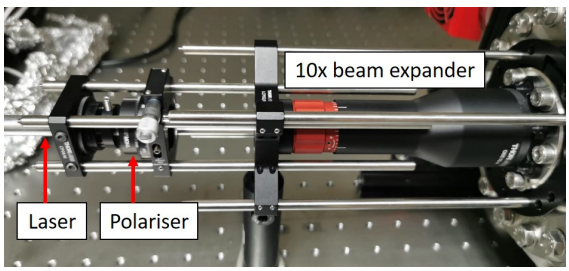

Figure 2: Upstream optical components: 532 nm laser, polariser, beam expander.

The previous experiment [10] encountered issues in imaging gas jets on the micrometre scale. Therefore, the updated system was designed to include a microscope for highly increased magnification. The downstream optics were changed, as shown in Fig. 3. The focusing lens was reduced to a 40 mm focal length, and a microscope objective lens and tube lens have been introduced after the Wollaston prism. With the microscope in place, the system had a magnification factor of 40.

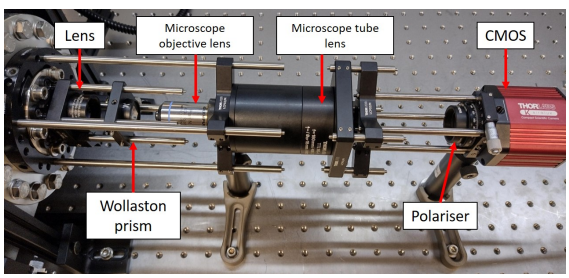

Figure 3: Downstream optical components: focusing lens (f = 40 mm), Wollaston prism, microscope objective and tube lens, polariser, CMOS.

The Wollaston prism was adjustable across a range of 50 mm, which was used to vary the fringe spacing (δ_f) via Eq. (3).

$$\delta_f = \frac{\lambda b}{\epsilon a} \tag{3}$$

Whilst the laser wavelength (λ) and separation angle of the Wollaston prism (ϵ) are fixed, the distance between the prism and lens (a) or prism and imaging plane (b) can be changed until the fringe spacing and number of visible fringes is suitable for imaging.

The vacuum chamber housing the gas jet nozzle sustained a pressure of 10^{-6} mbar, allowing for a high pressure gradient between the background and gas jet pressure of 0.5–2 bar. The nozzle used in this system had a 30 µm throat. The nozzle holder was mounted on an XYZ translation stage which could be operated from outside the chamber. This meant that the nozzle could be moved and aligned without breaking the vacuum. As with the previous experiments, nitrogen gas was used. This was both due to its usage in the BGC project which this interferometer is being designed for, but also to allow for straightforward comparison between both interferometer designs. A solenoid valve was used to control the gas jet, and run times varied between 0.1 and 1.5 s. Although longer period gas jets would likely have improved the results gained, the small size of the vacuum system meant that time and pressure constraints were in place to protect the turbomolecular pump.

RESULTS AND DISCUSSION

Figure 4 shows a comparison between an interferogram from the initial system (Fig. 4a) and the updated system (Fig. 4b). The interferogram from the previous version covers a region of 7 mm from the nozzle, and has a fringe spacing of 55.2 µm. The interferogram from the current system with the integrated microscope covers a region of only 200 µm from the nozzle, and has a fringe spacing of ~ 25 µm. Given that simulations of the phase shift for the gas jets used (Fig. 5) show the phase would only be visible within the first 30 µm, the reduced region of interest of the updated system is not an issue. Its ability to image a smaller area with smaller fringes allows for the resulting interferograms to image in much greater detail.

Figure 5 shows how the phase shift of the gas jet changes across a distance of 2 mm from the nozzle. It was calculated using Eq. (4) [12] to gain a density profile across this region, and then Eq. (2) to find the corresponding phase shift

$$\rho \approx 0.15\rho_0 \left(\frac{0.74d}{x \tan\theta} \right)^2 \tag{4}$$

where density (ρ) is given in m^{-3}, ρ_0 is the density at a point before the gas jet nozzle, d is the nozzle diameter (30 µm), θ is the half angle of the nozzle (45°), and x is the lateral distance from the nozzle throat. For these calculations, x was varied from 0 to 2000 µm.

The minimum phase shift of 12.8 mrad [10] is shown in red, and only sections of the plot above this would be visible to the system. This phase shift ($\Delta\phi_{min}$) is calculated via Eq. (5), utilising the pixel size of the CMOS camera (Δ = 3.45 µm) and setting the maximum fringe width (δ_f) needed to gain 5 fringes across the interferogram. This means that for a 5 bar jet, the phase shift would only be visible within the first 30 µm.

ISBN: 978-3-95450-215-8 ISSN: 2226-0366 doi:10.18429/JACoW-LINAC2022-MOPORI06

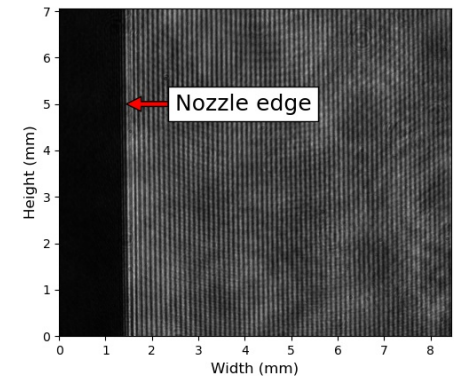

(a)

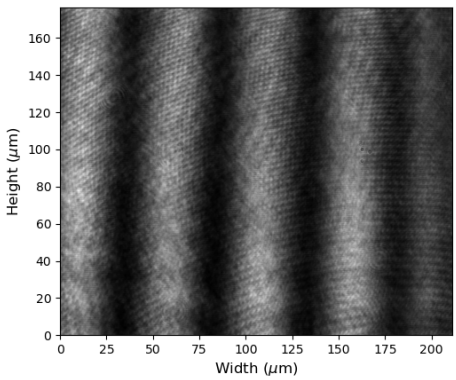

(b)

Figure 4: Interferograms from the initial (4a) and updated (4b) interferometer systems.

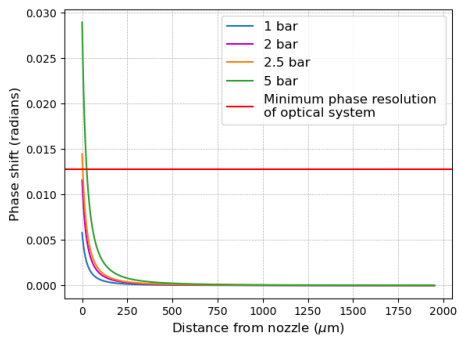

Figure 5: Calculated phase shift for N_2 jets at pressures 1–5 bar for a distance of 2000 µm from the nozzle. System phase resolution shown in red.

$$\Delta\phi_{min} = 2\pi\frac{\Delta}{\delta_f} = 12.8\,\text{mrad} \tag{5}$$

While the system has a theoretical phase resolution of 12.8 mrad, the interferograms produced have a different resolution. The system resolution ($\Delta\phi_S$) is given by the limits of the optical components, whilst the interferogram resolution ($\Delta\phi_I$) is given by the magnification and number of fringes. The aim of integrating the microscope in this interferometer was to reduce the phase resolution to be as close to the system resolution as possible. The resolution of interferograms gained from the initial system ($\Delta\phi_{I1}$) was calculated using Eq. (5). The fringe spacing was specified by the calculated phase shift being above $\Delta\phi_S$ for the first 30 µm after the nozzle across 5 fringes, giving δ_f as 6 µm. From Eq. (5), $\Delta\phi_{I1}$ was found to be 3613 mrad.

For the updated system, the phase resolution of the interferograms is given by Eq. (6), where M is the system magnification.

$$\Delta\phi_{I2} = \frac{\Delta\phi_{I1}}{M} = 90.325\,\text{mrad} \tag{6}$$

As both systems had interferogram resolutions much larger than the system resolution, it was not possible to image the phase shift which was occurring. In order to create interferograms with a resolution equal to 12.8 mrad, a magnification of 282.3 would be needed. This amount of magnification would be unrealistic to add to an interferometer for several reasons, mainly the issues it would cause with aligning and focusing the optical system. With the current set up having a magnification of 40, alignment was already a challenging procedure due to the field of view being in the order of micrometres.

CONCLUSIONS

This contribution described the updated design of a Nomarski style interferometer with integrated microscope and its applications in measuring density profiles of supersonic gas jets. Interferograms resulting from this updated system have been compared to the previous system, showing the field of view has reduced from 7 mm to around 200 µm, allowing for a much higher level of detail to be captured. The phase resolution of the resulting interferograms has been reduced from 3613 mrad to 90.325 mrad, although the theoretical system resolution of 12.8 mrad has still not been achieved. The next work for this project will involve increasing the phase shift and density of the gas jets in order to acquire measurements that can be processed at the current interferogram phase resolution. This will be done by increasing the gas pressure and nozzle size used. Whilst this contribution did not present interferograms which could be utilised to gain density profiles, it has placed lower bounds on the applicable parameter space of interferometery within gas jet instrumentation.

ACKNOWLEDGEMENTS

This work is supported by the AWAKE-UK phase II project grant No. ST/T001941/1, the STFC Cockcroft core grant No. ST/G008248/1 and the HL-LHC-UK phase II project funded by STFC under Grant Ref: ST/T001925/1.

ISBN: 978-3-95450-215-8 ISSN: 2226-0366 doi:10.18429/JACoW-LINAC2022-MOPORI06

REFERENCES

[1] H. Zhang *et al.*, "Development of supersonic gas-sheet-based beam profile monitors," 2019, WEPGW096. doi:10.18429/JACOW-IPAC2019-WEPGW096

[2] H. Zhang *et al.*, "Commissioning of a gas jet beam profile monitor for ebts and lhc," 2022, pp. 393–396. doi:10.18429/JACOW-IPAC2022-MOPOPT056

[3] R. Veness *et al.*, "Design of a prototype gas jet profile monitor for installation into the large hadron collider at cern," 2022, pp. 363–366. doi:10.18429/JACOW-IPAC2022-MOPOPT048

[4] A. Salehilashkajani *et al.*, "A gas curtain beam profile monitor using beam induced fluorescence for high intensity charged particle beams," *Applied Physics Letters*, vol. 120, p. 174 101, 17 2022. doi:10.1063/5.0085491

[5] O. Stringer, N. Kumar, C. Welsch, and H. Zhang, "A gas jet beam profile monitor for beam halo measurement," 2022, pp. 389–392. doi:10.18429/JACOW-IPAC2022-MOPOPT055

[6] M. Martinkova, M. Kalal, and Y. J. Rhee, "Compact design of a nomarski interferometer and its application in the diagnostics of coulomb explosions of deuterium clusters," *J. Phys.: Conf. Ser*, vol. 244, p. 32 053, 2010. doi:10.1088/1742-6596/244/3/032053

[7] J. J. Fendley, "Measurement of refractive index using a michelson interferometer," *Physics Education*, vol. 17, p. 209, 5 1982. doi:10.1088/0031-9120/17/5/001

[8] S. Sugawara, S. Nakao, Y. Miyazato, Y. Ishino, and K. Miki, "Three dimensional reconstruction of a microjet with a mach disk by mach–zehnder interferometers," *Journal of Fluid Mechanics*, vol. 893, p. 25, 2020. doi:10.1017/JFM.2020.217

[9] Q. Liu *et al.*, "Application of nomarski interference system in supersonic gas-jet target diagnosis," *AIP Advances*, vol. 11, pp. 1–7, 1 2021. doi:10.1063/5.0027317

[10] C. Swain, O. Apsimon, A. Salehilashkajani, C. Welsch, J. Wolfenden, and H. Zhang, "A modified nomarski interferometer to study supersonic gas jet density profiles," 2022, pp. 385–388. doi:10.18429/JACOW-IPAC2022-MOPOPT054

[11] E. Hecht, *Optics*, 4th ed. Addison-Wesley, 2002, pp. 623–639.

[12] A. Adelmann *et al.*, "Real-time tomography of gas-jets with a wollaston interferometer," *Applied Sciences (Switzerland)*, vol. 8, pp. 1–21, 3 2018. doi:10.3390/app8030443

[13] A. D. Buckingham and C. Graham, "The density dependence of the refractivity of gases," *Proceedings of the Royal Society of London. Series A, Mathematical and Physical Sciences Vol. 337, No. 1609*, pp. 275–291, 1974.

[14] M. Patel, J. Thomas, and H. C. Joshi, "Flow characterization of supersonic gas jets: Experiments and simulations," *Vacuum*, vol. 192, 2021. doi:10.1016/j.vacuum.2021.110440